



In-plane capacity of existing post-WWII beam-and-clay block floor systems

Alessandra Marini¹ · Andrea Belleri¹ · Chiara Passoni¹ · Francesca Feroldi² · Ezio Giuriani²

Received: 23 July 2021 / Accepted: 5 December 2021
© The Author(s) 2022

Abstract

A growing attention has been paid to the deep renovation of RC buildings, particularly focusing on their structural vulnerability and on the development of retrofit strategies; however, the issue of the in-plane diaphragm action and the capacity of existing floors has rarely been addressed. Although floor capacity does not seem critical for the seismic capacity of existing structures, commonly affected by greater vulnerabilities, it may become critical when an additional lateral force resisting system is introduced. This paper investigates the in-plane capacity of beam and hollow-clay-block floor system, typical of the European post-WWII RC buildings. Considering the diaphragm action as associated with an in-plane tied-arch mechanism developing within the floor thickness, the main failure mechanisms are discussed, and some simplified equations are provided to preliminary estimate the maximum capacity of floors. Experimental and numerical analyses are then carried out to validate the simplified analytical model. The relevant influence of possible staircase openings on the in-plane load paths and on diaphragm flexibility and capacity are also considered. Finally, the influence of the floor capacity on the seismic vulnerability assessment and in the conceptual design of a seismic retrofit intervention is discussed. This preliminary study shows that only some of the beam-and-block floor systems have a reliable in-plane capacity, while other typologies cannot serve as floor diaphragms. When the diaphragm action can be relied upon, the diaphragms often exhibit a fairly stiff behaviour up to a brittle failure, which is commonly associated with the ultimate capacity at the tied-arch supports.

Keywords Floor diaphragms · Beam and block floor system · Floor in-plane capacity · Existing post-WWII RC buildings · Seismic retrofit · Seismic vulnerability

1 Introduction

About half of European RC buildings were built in the aftermath of the WWII in the lack of seismic regulations. Today, their nominal structural service life is exhausted, and they are obsolete and intrinsically vulnerable to seismic actions. According to the UN Agenda

✉ Andrea Belleri
andrea.belleri@unibg.it

Extended author information available on the last page of the article

(United Nations 2015), a major effort should be made to retrofit these building stock in order to increase safety and resilience of the society.

For the retrofit of RC structures, great attention has been paid to structural vulnerability assessment and many seismic retrofit solutions have been proposed and validated throughout the years; however, the issue of the in-plane capacity of existing floors has rarely been addressed. In the seismic retrofit of buildings, floors play a critical role since they should be able to act as diaphragms connecting the vertical elements (frame elements or walls), thereby enabling the activation of the Lateral Force Resisting System (LFRS). In the response of a structure against earthquakes, the major roles of the floor diaphragms are the following (Mohele et al. 2010) (Fig. 1):

- To transfer the inertial loads from the floor to the vertical elements of the LFRS;
- To distribute the ‘transfer forces’ among different elements of the LFRS (Fleischman et al. 2005a). ‘Transfer forces’ (or ‘compatibility forces’) are internal actions that develop in the diaphragms in response to displacement incompatibilities in the LFRS (e.g. in dual systems composed of walls and frame) or to discontinuities of the vertical elements of the LFRS (e.g. in case of a setback of the building profile, podium structures, discontinuous walls between adjacent floors, etc.) (Bull 2004, Mohele et al. 2010) and may be even much larger than inertial forces (Gardiner et al. 2008);
- To provide lateral constraint to the vertical elements against buckling and second-order forces;
- To resist out-of-plane forces of exterior walls and claddings;
- To support soil loads below grade bearing out-of-plane against the basement walls, which are constrained at the diaphragm level.

In the design of seismic retrofit interventions, a doubt arises about the capacity of the existing flooring systems to act as diaphragms. In fact, although these systems do not seem critical for the capacity of the existing structures, which are often affected by vulnerabilities associated with the LFRS vertical elements, they may become critical when an additional stiff LFRS is provided to the structure. This issue is particularly relevant when retrofit interventions are applied from the outside of the building by means of structural exoskeletons, suitable to avoid inhabitants’ relocation and building downtime (Marini et al. 2017; Passoni et al. 2020). In this case, in fact, it is impossible to increase the in-plane floor capacity with traditional strengthening measures, i.e. casting an additional topping to the floor, since it would require the inhabitants’ relocation and the floor finishing substitution (FEMA 547, Marini et al. 2010, Mohele et al. 2010).

In order to evaluate the in-plane capacity of floor systems, some research was developed in recent years, particularly focusing on the seismic behaviour of the diaphragms. These studies mainly addressed different floor technologies, typical of the United States and

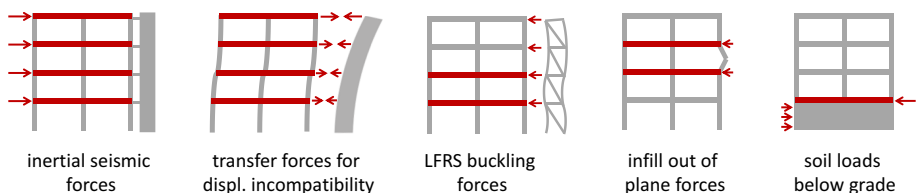


Fig. 1 Major roles of diaphragms to resist lateral loads

New Zealand construction sector, which are cast-in-place RC floors (Mohele et al. 2010, Correal et al. 2020), precast concrete floors (Fleischman et al. 2005a b; Schoettler et al. 2009; Zhang and Fleischman 2016; Bull 2004; Matthews 2005), and timber diaphragms (Moroder et al. 2014; Moroder 2016; Brandner et al. 2017). To the best of the authors' knowledge, only a few researches were carried out on beam-and-block floor systems (Tena-Colunga et al. 2015; León Flores et al. 2008; Pecce et al. 2017); however, the considered systems differ from the post-WWII European beam-and-clay block floors because they were realized with concrete blocks, they always presented a cast-in-place reinforced concrete overlaying thin slab, and they were designed in accordance to modern building codes.

This research investigates the in-plane capacity of existing beam-and-clay block floor systems typical of post-WWII European RC buildings. Focusing on the sole inertial forces, internal load paths in the diaphragms are investigated, and possible failure mechanisms of beam-and-clay block floors are discussed. In particular, if some prerequisites are ascertained, a tied-arch resistant mechanism and a stiff behaviour up to a brittle failure is proposed to preliminary model the structural behaviour and to estimate the ultimate capacity of these floors. The model is validated by means of experimental and numerical analyses. A preliminary laboratory test is carried out to determine the mechanical properties of a sub-system composed by a clay block and the two adjacent RC joists when subjected to a biaxial stress state. Experimental results are then implemented into a bidimensional non-linear finite element model of the diaphragm, considering the floor in the as-is and in two different retrofit configurations (i.e. resulting in different diaphragm span to width ratios—adding 2 or 4 transversal shear walls) and subjected to a uniform distribution of inertial forces. These analyses allow to validate the proposed diaphragm internal load paths and the associated diaphragm ultimate capacity for varying the mechanical properties of the system and for varying the retrofit configurations. Finally, the implications of such study for the design of seismic retrofit interventions, especially when carried out from outside, are discussed.

2 Typologies of beam-and-clay block floor systems

Two main floor typologies can be found in European post-WWII RC buildings: RC slabs and one-way composite beam-and-clay block floor systems. Typical one-way beam-and-block floor systems, particularly widespread over the Mediterranean countries, are made of a series of parallel joists and rows of hollow-clay-blocks, sometimes completed with a RC topping of 2–5 cm thickness. In those years, each brick manufacturer developed different patented systems leading to a variety of floor typologies, but with similar features.

Joists may be either cast-in-place RC beams, often featuring a lower clay formwork, or prefabricated RC beams, made of mixed masonry and RC elements or by pre-stressed RC joists. They generally have a base ranging between 70 mm–100 mm, with a height-to-span ratio of about 1/30, as typically requested in standards at the time of construction (as, for instance, Oliveto et al. 2011).

Hollow-clay-blocks, adopted for their lightweight properties and for their low cost, are either single blocks (Fig. 2a, b) or an assemblage of different hollow-clay-tiles (Fig. 2c, d). Special hollow-clay-blocks with a thickened top were also developed to contribute to the structural capacity of the floors against gravity loads (Fig. 2b). With these special blocks, the concrete topping was often avoided since the thickened top of the block (Fig. 2b) was considered to contribute to the flexural resistance of the floor. The type of blocks and the

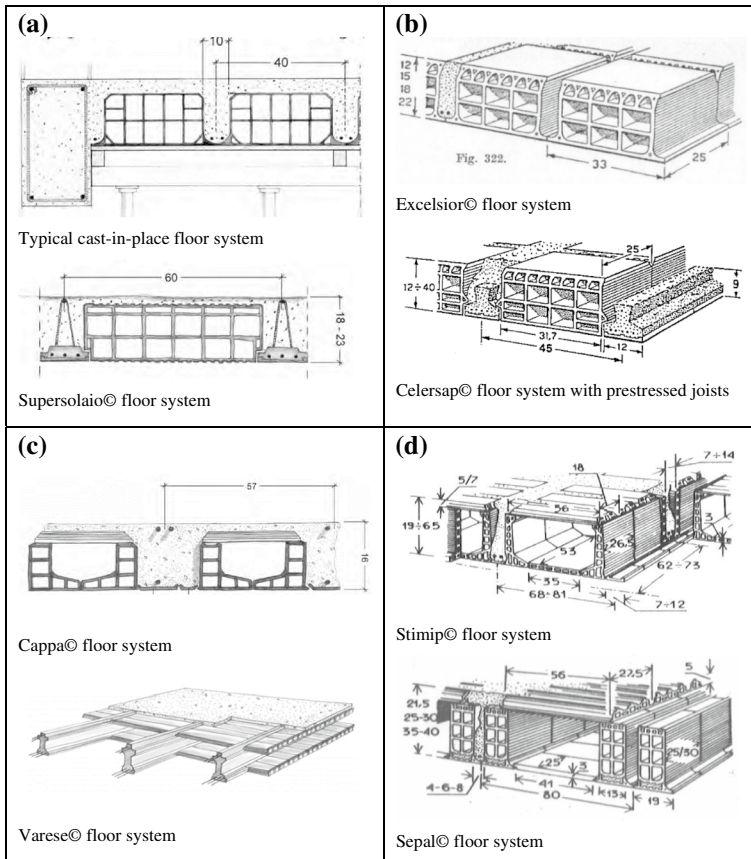


Fig. 2 Typical one-way beam and hollow-clay-block floor systems with (a) and without (b) concrete topping; beam and hollow-clay-block floor systems with blocks composed of different hollow-clay elements with (c) and without (d) concrete topping. (Iurcotta 1968, RDB 1950, ANDIL 1983). Adapted from Zanotti et al. (2014)

presence of the concrete topping slab are critical for the estimate of the in-plane floor capacity.

3 In-plane load path and failure mechanisms

Over the years, the in-plane capacity of the floor systems, and the analysis of the seismic load path in the diaphragms have been studied by several researches with reference to different floor typologies. Approaches to evaluate internal load paths may vary from simplified analytical models to finite element analyses. The complexity of the model is often a function of the regularity of the floor system. When the building is regular in plan, the simplest model to represent internal diaphragm forces is the so-called ‘equivalent deep beam analogy’ (Bull 2004; Mohele et al. 2010). In this model, the inertia forces of the floor are represented as distributed forces along the diaphragm span, which cause in-plane compression struts in the diaphragms arching to the supports and balanced by a tension chord or

tie along the bottom edge of the diaphragm (Bull 2004). The capacity of the diaphragms is thus connected to a ‘tied-arch’ resisting mechanism. When the diaphragms feature plan irregularity, particularly in the case of large opening in the diaphragms, the more complex strut-and-tie approach should preferably be adopted in order to determine the statically admissible load paths in the diaphragm (Bull 2004). Finally, for increasing complexity of the floor irregularities and for irregular LFRS, equivalent truss method (Moroder 2016) or finite element modelling should be addressed. The finite element modelling is also an effective method to compute the ‘transfer forces’ between the diaphragm and the vertical elements of the LFRS (Mohele et al. 2010).

Previous researches investigated the possible influence of the diaphragm flexibility on the load paths due to the variation of the dynamic properties of a structure and many studies were devoted to the classification of existing floor systems among rigid, semi-rigid or flexible floors (Tena-Colunga et al. 2015; Moroder 2016, Pecce 2019, among others). In the following, the in-plane capacity of a general beam-and-clay block floor system is evaluated, also accounting for the influence of large openings.

3.1 Tied-arch mechanism in floor diaphragms

Considering the tied-arch resisting mechanism and a floor with regular geometry, the magnitude of the internal actions in the system for a given set of inertia forces depends on the tied-arch net span (L) and rise (z_d) (Fig. 3), which in turn depend on the internal load path in the floor. The span and rise of the tied-arch are influenced by the floor layout, by openings (i.e. the stairwells), and by the distance between adjacent vertical elements of the new and existing LFRS (Fig. 3).

When considering a typical post-WWII RC building in the as-is condition subjected to inertial forces, three main layouts of the LFRS may generally be considered (Fig. 3), resulting in different diaphragm’s load paths: (1) the RC frame structural system, where smaller tied-arches develop with span assumed equal to the spacing of the frame columns; (2) the infilled frame, where the tied-arch span is equal to the distance between the stiffer infilled frames (or to the infilled frames and the staircase walls); and (3) the frame with stiff staircase walls, where the reactions are taken by the walls and the loads are distributed so as to form two rampant arches having an extrados tie.

When retrofitting an existing building, different configurations of the new LFRS may be considered. In this paper, focus is made on a retrofit placed on the outside of the building, such as those implementing exoskeletons, which are aimed at minimizing the barriers to the renovation (Marini et al. 2017) and where the need of either floor strengthening or the construction of brand-new diaphragms inside the building would jeopardize the feasibility of the solution.

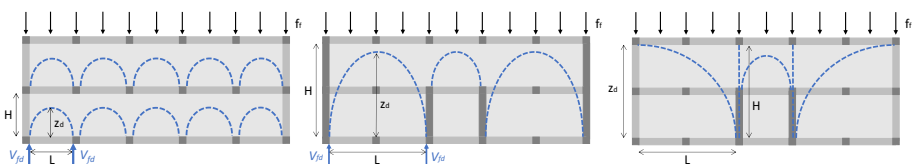


Fig. 3 Floor load distribution for three possible configurations of the building in the as-is situation in terms of geometry of the tied-arches. Note: for sake of clarity, the horizontal seismic loading is represented as external loads instead of distributed floor loads

In the conceptual design of the structural exoskeleton, two main typologies could be adopted: the shear wall and the shell solutions (Marini et al. 2017; Passoni et al. 2020). Considering the shear wall exoskeleton, a limited number of external walls are added to the existing building. The new retrofit system could be made by traditional reinforced concrete (RC) walls, steel braces or steel plate shear walls (Riva et al. 2010; Moghimi and Driver 2013), post tensioned cross-laminated timber shear walls (Sustersic and Dujic 2014) or innovative systems such as rocking or hinged walls (Qu et al. 2012), among others. Considering the shell exoskeleton, new façades structural systems are exploited to enable a box-structural behaviour (Giuriani and Marini 2008; Giuriani et al. 2015). This leads to a reduced stress level in the new structural elements and in the foundation system and to a higher lateral stiffness compared to the shear wall solution. Some examples of shell exoskeletons are wooden shells (Zanni et al. 2020 2021), steel shells, or steel diagonal grid systems (diagrid exoskeletons) (Mele et al. 2021; Di Lorenzo et al. 2020; Labò et al. 2020), which may be in adherence of the existing building or may present an offset with respect of the building façades.

When the building is retrofitted by means of additional external LFRS, whose stiffness is higher than the stiffness of the existing building, the diaphragm tied-arch span is equal to the distance between the new seismic resistant elements (Fig. 4). In these cases, the tied-arch span usually increases in the post retrofit condition with respect to the as-is situation, especially when shell exoskeletons are applied, and the influence of the openings may become even more critical, as it may reduce the in-plane capacity of the diaphragm by reducing the tied-arch rise. In addition, higher inertia forces are expected in the stiffer retrofitted building.

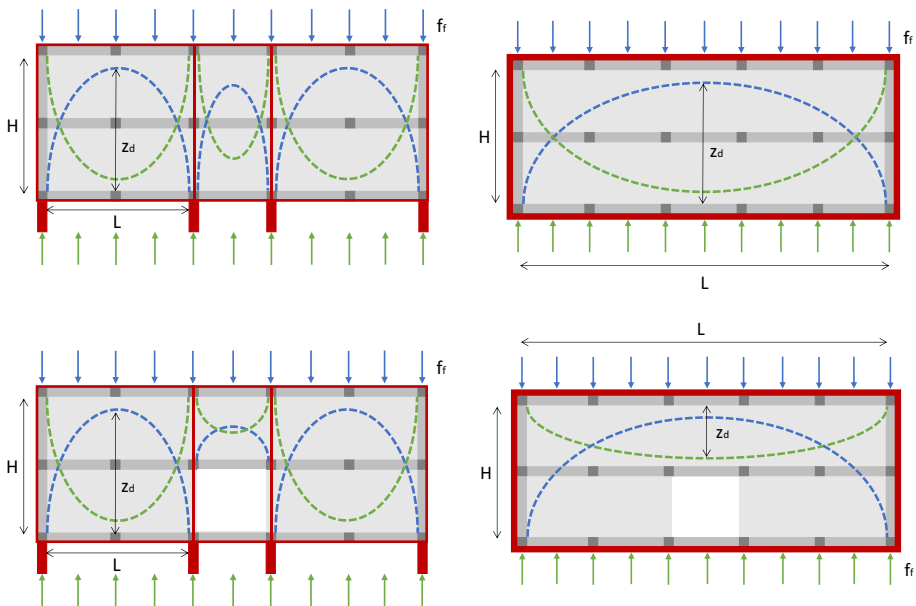


Fig. 4 Main floor load distribution for the retrofitted building with shear walls or with a shell configuration, not considering (*top*) or considering (*bottom*) a floor opening at the staircase, in terms of geometry of the tied-arches. Referring to the plan views of the floors, blue tied-arches are associated with downward actions; while green tied-arches to upward actions

3.2 In-plane failure mechanisms

When floor systems are made of different components (such as precast concrete units or beam-and-block elements), possible load paths may involve individual units and their joints and interfaces, and their potentially brittle behaviour may influence the global capacity of the system (Fleischman et al. 2005a).

Existing beam-and-clay block floor systems can be divided into two main categories: floor system featuring a thin structural overlay (or thin RC slab), and the floors lacking the overlay. In the case of cast-in-place structural topping, either featuring or lacking the steel reinforcement mesh, the loads are distributed between the concrete topping and the beam-and-block system as a function of their relative stiffness, up to the brittle failure of one of the layers, after which no redistribution of the internal actions can occur. On the other hand, in the worst case-scenario of beam-and-block floor systems lacking the topping overlay (Fig. 2b), the resisting arch must develop across the joists and the lightweight hollow blocks. In both cases, the effectiveness of the load transfer mechanism between the joists and the blocks and the possible activable failure mechanisms must be carefully assessed. For example, when single hollow clay blocks are substituted by an assemblage of hollow-clay-tiles simply supported by the joists and in the absence of the concrete topping (Fig. 2d), the system is unable to transfer in-plane actions.

When the diaphragm can be modelled with the tied-arch resisting mechanism, i.e. in case of systems with regular geometry, the floor in-plane capacity is related to the resistance of the single tied-arch. Considering, for sake of clarity, a uniform distribution of the seismic inertia loads f_f applied at the upper edge of the diaphragm (i.e. seismic action per unit length transferred across the floor diaphragm), the maximum lateral thrust (F_o) at the supports is equal to $f_f L^2/(8z_d)$, where L is the tied-arch net span and z_d is the arch rise (Fig. 5). The tied-arch's vertical reaction force at each support (V_f) is equal to $f_f L/2$, and the inclination angle (α) of the compressed strut at the supports is defined by the relationship $\tan\alpha = V_f/F_o$. At the supports, F_o is transferred by the contact between the RC joist and the blocks; while V_f by the shear action along the interface between the side beam and the blocks.

Three main vulnerable regions, which may exhibit different failure mechanisms, must be verified for the effective development of a tied-arch resisting system. Referring to the beam-and-block configuration of Fig. 5 (analogous considerations apply for beams-and-blocks spanning in the orthogonal direction), such failure mechanisms are located at:

1. The arch key section (Mechanism A), where the brick is compressed orthogonally to the direction of the hollows (hollow brick's weakest direction);
2. The tied-arch supports (Mechanism B), where combined compression and shear stresses are transferred. At this location, either the ultimate compression resistance in the hollow brick weakest direction, or the ultimate shear resistance of the hollow brick, or the shear resistance of the brick-to-concrete interface may be exceeded;
3. The tied-arch bottom chord (Mechanism C), where tensile failure of the "tie" may be triggered by overcoming the tensile resistance of the RC edge-beam, the adhesion at the brick-to-beam interface, or the brick tensile resistance.

The failure at the tied-arch supports (i.e. Mechanism B) often dominates the seismic ultimate response of heterogeneous beam-and-block floor systems lacking a RC overlay. Failure of the "tie" (i.e. Mechanism C) may also occur, but its resistance can be easily

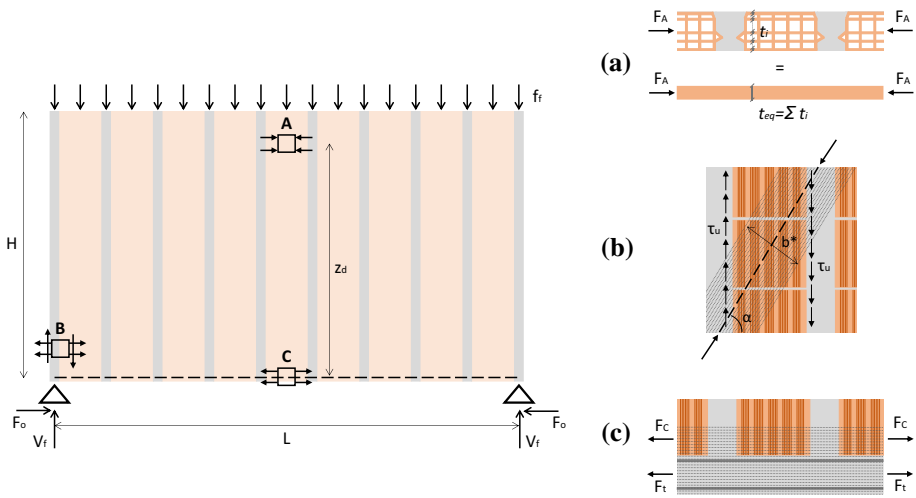


Fig. 5 Tied-arch mechanism activated within the floor depth and regions of possible failure of the tied-arch resisting system: **a** the arch key section, where the brick is compressed orthogonally to the direction of the hollows (the blocks are considered as an equivalent clay slab with thickness equal to the net thickness of the clay block horizontal webs); **b** the tied-arch supports where compression-shear failure may occur; **c** the tied-arch bottom chord, with possible overcoming of its tensile strength

increased by fixing additional steel stringcourses alongside the edge-beam. Mechanisms A is usually not critical for the diaphragm. The capacity of Mechanism A depends on the tied-arch net span, which in turn depends on the layout of the floor and on the influence of possible openings. Unless the opening extends over the whole depth of the floor, the strength of the arch at the key section is often not critical.

3.3 Design in-plane capacity of floors

The design in-plane capacity of the floor can be defined with reference to the simplified tied-arch model, with span length L , as the maximum reaction force at the tied arch support (V_{fd}), or as the maximum load per unit length transferred across the floor (f_{fd}):

$$V_{fd} = \min\{V_{fA}; V_{fB}; V_{fC}\} \tag{1}$$

$$f_{fd} = 2V_{fd}/L \tag{2}$$

where V_{fA} , V_{fB} and V_{fC} are the floor shear reactions associated with the onset of mechanisms A, B, and C, respectively. In the following, reference is made to beam-and-block floors with and without the concrete topping overlay under the hypothesis of uniform distributed loads.

3.3.1 Mechanism A

The in-plane capacity of the floor is limited by the crushing of the clay bricks loaded in the weakest direction (orthogonal to the brick hollows) at the arch key section. The maximum

axial force in the tied-arch at the key may be calculated as the minimum force that causes the collapse of the weakest layer, considering that the loads are divided in the blocks and in the concrete topping as a function of their stiffness and that it is a fragile mechanism:

$$F_A^{TOT} = \min \left[f_{c,b\perp} \left(A_b + \frac{E_c}{E_b} A_c \right); f_c \left(A_c + \frac{E_b}{E_c} A_b \right) \right] \tag{3}$$

where $f_{c,b\perp}$ is the maximum compressive strength in the brick weakest direction; f_c is the compressive strength of the concrete; E_b and E_c are the elastic modulus of the blocks and of the concrete topping; $A_b = t_{eq} b^*$ is the resisting area of the blocks considering a homogeneous equivalent brick slab with thickness t_{eq} , corresponding to the net thickness of the clay block horizontal webs (Fig. 5a), and width b^* is the maximum width of the arch developing in the floor, considered as the portion of the slab in which stresses are remarkable (herein tentatively assumed equal to 25–50 t_{eq} , based on the numerical analyses of Chapter 5; further validation is object of an ongoing research); and $A_c = t_c b^*$ is the resisting area of the concrete topping slab with thickness t_c and width b^* .

The related shear reaction force at the supports is:

$$V_{fA} = 4F_A^{TOT} \left(\frac{z_d}{L} \right) \tag{4}$$

where L and z_d are the tied-arch span and rise, respectively.

3.3.2 Mechanism B

The in-plane capacity of the floor is associated with the failure of the interface between the brick and the collector (either a RC beam or a floor joist), hence the failure is triggered for overcoming the maximum tensile stress at section B. The shear stress distribution is a function of the stiffness ratio between the collector and the diaphragm. The in-plane capacity may be calculated as the minimum force that causes the collapse of the weakest layer, considering that the loads are divided in the blocks and in the concrete topping as a function of their stiffness and that it is a fragile mechanism:

$$V_{fB} = \min \left[\frac{\tau_{ud} H}{\beta} \left(t_{eq} + \frac{G_c}{G_b} t_c \right); \frac{\tau_{cd} H}{\beta} \left(t_c + \frac{G_b}{G_c} t_{eq} \right) \right] \tag{5}$$

where τ_{ud} is the design ultimate shear stress of the brick element; τ_{cd} is the design ultimate shear stress of the RC topping slab overlay (the design values are obtained from dividing the characteristic values by a safety factor); G_b and G_c are the shear modulus of the blocks and of the concrete topping, respectively; H is the depth of the floor; β is a coefficient accounting for the shear stress distribution and it is defined as the ratio between the maximum and mean shear stress across the diaphragm depth. This coefficient is governed by the ratio between the axial stiffness of the collector and the shear stiffness of the diaphragm. In particular $\beta = 1.3$ (Leonhardt, 1979) if the axial stiffness of the collector is much higher than the shear stiffness of the diaphragm (as for instance assumed when the shear wall is aligned with a RC beam or ring beam), whereas $\beta = 2.0$ if the axial stiffness of the collector is lower than the shear stiffness of the diaphragm, in this case the shear stress follows an almost triangular distribution at the beam-to-floor interface. This aspect will be addressed in a following section (Sect. 5.3).

3.3.3 Mechanism C

The axial force in the tie is provided by the continuous longitudinal rebars and the concrete in tension in the edge beam, by a possible additional steel stringcourse (or by ring beams made with steel plates) located outside the building in correspondence of the edge beam (see Fig. 18), and by the bond between the clay blocks and the joists. Neglecting the last contribution, which is considered not reliable, the maximum axial capacity of the tie of the arch may be calculated considering two configurations: (1) at the concrete tensile failure ($F_{t,pre}$) and (2) after concrete cracking, at yielding of the steel elements ($F_{t,post}$). The floor capacity is associated with the maximum value (F_t) between $F_{t,pre}$ and $F_{t,post}$. Note that, if the concrete tensile strength is neglected, the sole $F_{t,post}$ may be considered. The maximum axial force at the concrete tensile failure may be calculated as:

$$F_{t,pre} = f_t \left(\alpha_1 A_c + \frac{E_s}{E_c} \alpha_2 A_s + \frac{E_s}{E_c} A_{Tie} \right) \quad (6)$$

where f_t is the concrete tensile strength; E_s and E_c are the elastic modulus of the steel and of the concrete, respectively; A_c is the concrete area of the edge beam; A_s is the amount of continuous longitudinal rebars in the edge beam; A_{Tie} is the area of possible additional steel stringcourses. This formula has been derived considering a beam under tensile axial load but could be generalized and applied also for continuous beams under flexure by introducing the reduction factors α_1 and α_2 , which, for instance, allow to consider the combined effects of the seismic tensile axial force and the bending moment due to gravity loads. A detailed treatment of such topic goes beyond the purpose of the paper.

The maximum axial force after the concrete tensile failure is:

$$F_{t,post} = f_{yd} \alpha_2 A_s + f_{ydTie} A_{Tie} \quad (7)$$

where f_{yd} and f_{ydTie} are the steel design tensile strength of the reinforcement and of the tie, respectively.

It is worth noting that these formulations do not account for the resisting contribution of those portions of the floor in close proximity to the arch tie, which could be relevant in the case of RC topping. The reaction force at the support is equal to:

$$V_{JC} = 4F_t \left(\frac{z_d}{L} \right) \quad (8)$$

4 Experimental tests on a floor sub-assembly

With reference to the tied-arch scheme in Fig. 5, focus was made on the possible failure occurring at the supports (Mechanism B), where the inclined strut converges into the support and the shear failure of the blocks may occur. For this purpose, the in-plane shear resistance of the brick-to-beam sub-system was preliminary assessed through an experimental campaign aimed at evaluating the shear capacity of single lightweight hollow blocks under minimum confining action. The results of the tests proved evidence that an in-plane tied-arch mechanism can develop within the floor, even in the case of floors lacking the concrete overlay, as long as the lightweight hollow blocks extend over the thickness of the floor (thus with the exception of floors in Fig. 2c, d).

The selected test specimen is a modular sub-assembly of the composite floor, composed by a single hollow brick and the adjoining concrete joists (Fig. 6). A single block, rather than a series of blocks, was selected to account for the common construction practice in which neighbouring blocks may be not in direct contact between each other (Fig. 5, mechanism B). Commercial hollow clay blocks were adopted in the experimental campaign (clay blocks $16 \times 40 \times 5$ cm for not composite action floor systems according to NTC 2018). Although current clay blocks have different shapes and sizes compared to those used in post-WWII existing buildings, the inherent mechanical properties of the material and the production methods have remained almost unchanged over time, except for the most stringent quality controls. The mechanical properties of the tested hollow clay blocks are reported in Table 1 and compared with the corresponding characteristic values provided by the producer. The side joists were made by C20/25 concrete (i.e. characteristic cubic compressive strength at 28 days greater than 25 MPa), compatible with an average quality concrete at the time of construction.

A specific testing frame was conceived to replicate the actual compression-shear biaxial stress state on the tested specimen (Fig. 6). The specimen sides were firmly connected to rigid steel frames and the alignment of the applied load (F) with the sub-assembly centroid axis was guaranteed (Fig. 6c). As a result, an almost uniform shear stress distribution, together with a bending moment (Fig. 6b), was transferred along the clay-block to concrete interface. The bond between the sample and the steel frames was improved by welding 5 mm diameter steel bars on the side plates of the frames. The confining load (Fig. 6) was provided by horizontal threaded bars and controlled by a stack of cup springs placed at the head of each bar.

The instrumentation setup consisted of a load cell to measure the applied load (F) and of displacement transducers to monitor the horizontal and vertical relative displacement of the rigid steel frame and the confining load level in the horizontal bars.

Three tests were conducted. In the initial loading step, the confining pre-stress action was applied to the specimen through the tightening of the threaded steel bars; then the

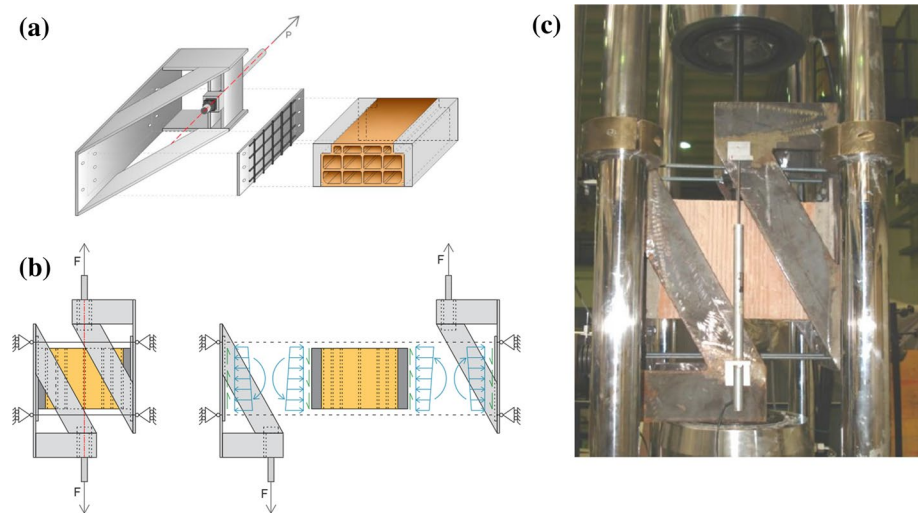


Fig. 6 Modelling of the experimental test: selection of the floor sub-assembly (a); applied load and internal actions along the clay-bloc to joist interfaces (b); experimental test set-up (c)

Table 1 Mechanical properties of the hollow clay bricks adopted in the experimental tests (block for mixed slab $16 \times 40 \times 25$ cm): comparison of the average values obtained on 8 standard tests and the ones declared by the producer

| | Average on 8 standard tests (MPa) | From the producer (MPa) |
|---|-----------------------------------|-------------------------|
| compression resistance parallel to the voids ($f_{c\parallel}$) | 39.5 | 25.7 |
| compression resistance orthogonal to the voids ($f_{c\perp}$) | 18.7 | 11.1 |
| flexural tensile strength ($f_{c,flex}$) | 14.7 | 11.2 |

vertical load was applied in displacement control. The increase of the applied vertical displacement led to an increase of the bending moment at the specimen sides (Fig. 6b), which was associated with tensile stresses. As tensile stresses increased, cracks were triggered along the specimen-to-frame interfaces and partial detachment was observed. The specimen started to rotate pushing against the steel frames, thereby increasing the tension in the confining bars and therefore the confining pressure. No significant deformations were observed until overcoming the initial confinement stress; beyond such value, cracks propagated in the concrete matrix, the contact area reduced, and the rotation of the specimen became significant. Beyond an initial setback, the load increased until the brittle shear failure of the clay block, which occurred with a large inclined crack (Fig. 7).

The load–displacement curves of the tested specimens are shown in Fig. 7, while the results are reported in Table 2. The ultimate shear strength (Table 2) was evaluated by assuming the maximum applied load as balanced by an equivalent uniform shear stress distribution along the clay block net cross Sect. (8750 mm^2). The ultimate shear resistance was in the range $1.7 \div 2.0$ MPa. The minimum value is considered for conservative estimates in the following numerical simulations.

5 Numerical study on the in-plane diaphragm capacity

A numerical model was developed to further investigate the in-plane performance of existing floors lacking concrete topping. Reference was made to a $25 \text{ m} \times 10 \text{ m}$ composite beam-and-clay block floor of a typical Post-WWII building, featuring a $5 \text{ m} \times 5 \text{ m}$ column grid. The floor was considered as isolated from the building. A sensitivity study was carried out by varying a set of relevant parameters, including material properties, structural details, boundary conditions and geometric features. In this preliminary study the following simplifications apply: the stairwell floor opening is initially neglected, only the perimeter beams are considered, and only inertia loads along the transverse direction are applied.

A two-dimensional model (Fig. 8) was assembled and nonlinear numerical analyses were carried out to assess the in-plane resistance of the floor system. The FEM code Abaqus (ver. 6.11, 2011) was adopted (Dassault Systèmes Simulia 2011). Given the demonstrative purpose of this preliminary analysis, homogeneous equivalent inelastic material properties were considered (Table 3). This hypothesis is quite simplifying of the actual floor in-plane behaviour, which is highly orthotropic, given the heterogeneity and directionality of the floor components, but it allows describing the overall floor

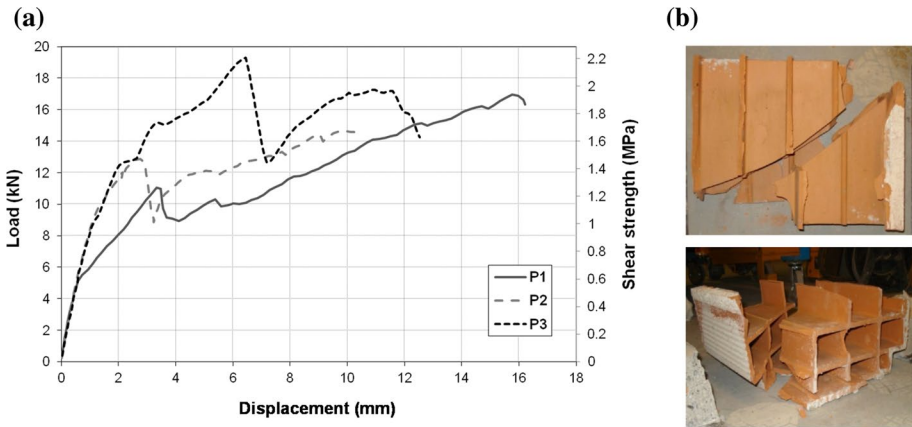


Fig. 7 a Experimental load–displacement curves for increasing values of the confining load; b shear failure of the clay blocks

Table 2 Shear test results

| Test id | Initial confinement (kN) | Confinement at failure (kN) | Ultimate load (kN) | Ultimate shear strength (MPa) |
|---------|--------------------------|-----------------------------|--------------------|-------------------------------|
| P1 | 4 | 18 | 16.9 | 1.9 |
| P2 | 10 | 16 | 14.7 | 1.7 |
| P3 | 20 | 22 | 17.2 | 2.0 |

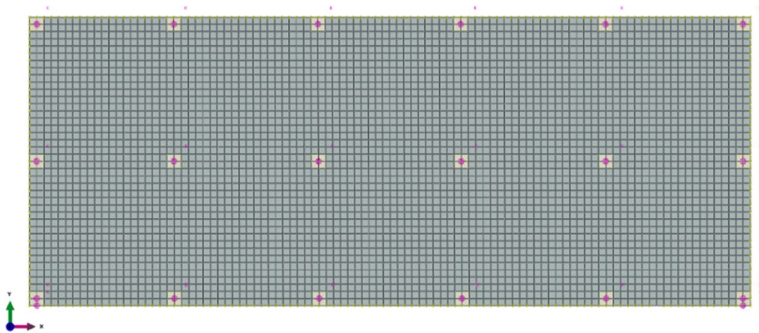


Fig. 8 Finite element mesh

behaviour analogously to what done dealing with masonry following a macro-modeling approach (e.g. Lourenco 1996; Milani et al. 2006a and 2006b). A smeared crack model was adopted to describe the fracture process. Such model, referred to as “concrete damage plasticity”, provides a general capability for modeling quasi-brittle materials in structures subjected to monotonic, cyclic, or dynamic loading. The failure stress corresponds to the onset of micro-cracking, beyond which further micro-cracks development is represented macroscopically with a softening stress–strain response inducing strain

Table 3 Material properties

| | | |
|--|----------------------------------|-----------------|
| Equivalent homogeneous material for plate elements | Elastic modulus, $E_{c,e}$ | 23000 MPa |
| | Poisson coefficient, $\nu_{c,e}$ | 0.2 |
| | Compressive strength, $f_{c,e}$ | 8 MPa |
| | Tensile strength, $f_{t,e}$ | 0.5–1.0–2.0 MPa |
| Concrete damage plasticity parameters | Dilation angle, φ | 31 |
| | f_{bd}/f_{co} | 1.0 |
| | K | 0.667 |
| | Viscosity parameter | 0.0004 |
| RC Edge beam | Elastic modulus, E_c | 30000 MPa |
| | Poisson coefficient, ν_c | 0.2 |
| | Compressive strength, f_c | 20 MPa |
| | Tensile strength, f_t | 0.75 MPa |

localization. The “Static-Riks” (Dassault Systèmes Simulia 2011) type of analysis was selected for the loading increment procedure. This type of analysis uses an arc-length method to determine the response of the loaded structure, and it is particularly suitable when a significant change of the structural stiffness is expected.

In an attempt to capture all the basic failure modes (A, B, C in Fig. 5), the properties of the equivalent homogeneous material were initially set to the minimum values of the specific properties of the component materials (i.e. blocks, beams and beam-block interface): the compressive strength ($f_{c,eq}$) was set equal to the block compressive strength in the weakest direction, which may govern failure at the tied-arch key in compression (point A, Fig. 5); the tensile strength ($f_{t,eq}$) was calibrated to determine the shear resistance measured in the experimental tests, so as to capture shear failure at the supports (point B, Fig. 5).

The floor was modelled with 4-node shell elements (S4R element in Abaqus) with a size of 0.25 m, selected after a sensitivity analysis to avoid mesh dependency. The thickness of the equivalent plate was set equal to 35 mm, corresponding to the net thickness of the thin webs of the clay block withstanding shear stresses. The homogeneous equivalent material was assumed as elastic-perfectly plastic in compression, while a softening behaviour was introduced in tension to account for crack onset upon exceeding the tensile resistance. To this end, the nonlinear tension law implemented in the concrete damage plasticity model (Table 3) was adopted with a multi-linear softening law (Fig. 9a).

The elements overlaying the column cross-section were considered elastic. The RC edge beams (0.6 m × 0.3 m) were modelled with 2 nodes truss elements (T3D2 element in Abaqus) to avoid accounting for their shear contribution; a length equal to 0.25 m was selected. C20/25 concrete was considered, and non-symmetrical elastic-perfectly plastic law was adopted to model the material in uniaxial compression and tension (Table 3). Ordinary steel reinforcement (Type Aq42, referring to Post-WWII Italian standards) in the longitudinal side beams was represented with two-node embedded reinforcing elements (total cross section equal to 500 mm²). The amount of steel reinforcement (0.2% A_c) was selected as an estimate of the available continuous longitudinal reinforcement suitable for tie action. Compressive and tensile behaviour of the steel is described with a symmetrical elasto-plastic law, with yielding stress equal to 235 MPa, elastic modulus 210000 MPa, post-yield modulus equal to 1800 MPa and post-yield capacity equal to 360 MPa.

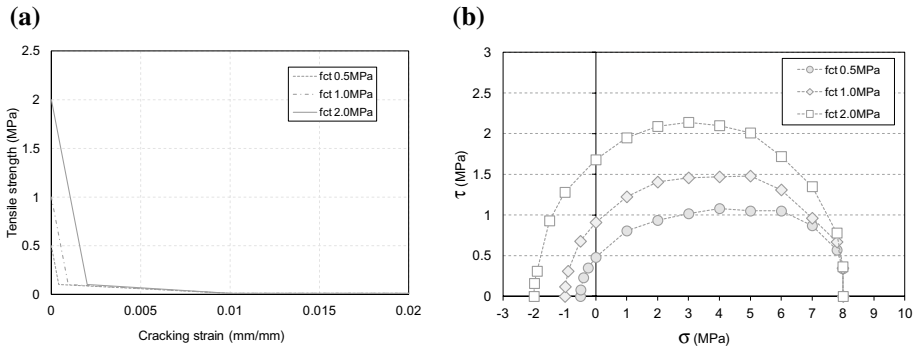


Fig. 9 **a** Post-cracking tensile law for concrete; **b** bi-axial τ - σ domain for concrete

The in-plane load was uniformly distributed along the diaphragm surface and monotonically increased up to collapse. Two main scenarios were considered: the “AS-IS” condition, and the “RETROFIT” condition, in which new seismic resistant walls were added at the floor ends (Fig. 11a). The floor diaphragm was elastically supported at each column in the AS-IS scenario, and on the new additional seismic resisting elements in the RETROFIT scenario. The first set of analyses did not consider the influence of possible floor openings (e.g. stairs well); indeed, significant floor openings, which may hamper the efficiency of the diaphragm action, are addressed in the Sect. 5.2.

Sensitivity analyses were carried out for both scenarios by varying the material properties and the geometry of the floor components, in particular:

1. The shear strength and the related tensile strength of the equivalent homogeneous plate: $\tau = [0.5 \ 0.9 \ 1.7]$ MPa, corresponding to $f_{ct} = [0.5 \ 1.0 \ 2.0]$ MPa, respectively (Fig. 9);
2. The additional steel tie applied as an external stringcourse to the edge-beams: $A_{Tie} = [0 \ 5 \ 15 \ 25]$ cm².

In the analyses, the reference values of the parameters are: $\tau = 1.7$ MPa (corresponding to the minimum shear stress obtained from the experimental tests), $A_s = 5$ cm², $A_{Tie} = 0$ cm², elastic stiffness of the spring modelling the lateral stiffness of each column equal to 4.5 kN/mm (corresponding to the stiffness of a 0.3m×0.3m×3m column in double bending), sum of the elastic stiffness of the springs modelling the new additional lateral seismic resisting elements equal to 162 kN/mm (corresponding to twice the lateral stiffness in the AS-IS condition, as recommended by previous studies: Marini et al. 2017; Labò et al. 2020; Feroldi 2014). The boundary conditions were provided by the elastic springs of the columns and by the additional resisting elements, which are fixed to the ground.

5.1 Floor in-plane performance in the AS-IS and RETROFIT configurations

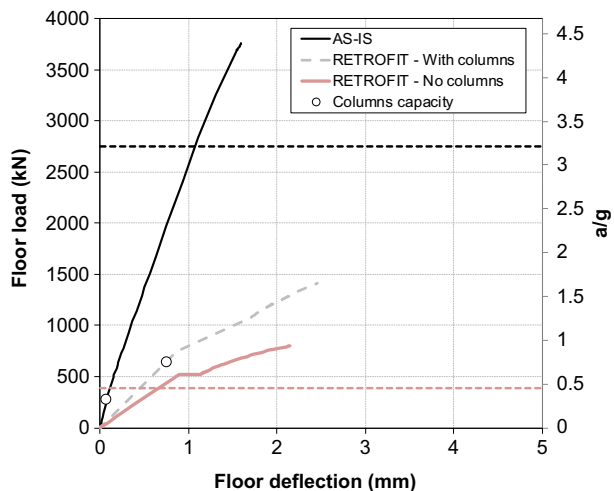
Figure 10 shows the floor load versus the floor mid-span net deflection (diaphragm maximum displacement minus diaphragm side displacement) in both scenarios. The net mid-span deflection is evaluated with reference to the floor lower corners. In the AS-IS condition, the response curve is linear elastic, provided that in-plane stresses never exceed the elastic limit even for high applied in-plane loads. This is basically due to the reduced span

(and relatively reduced span to rise ratio) of the activated natural arches, bridging the span between adjacent columns and transferring the floor in-plane actions. Figure 11b and c display the plastic deformations and the principal compression stresses within the floor. The activation of the tied-arch mechanism can be observed. The failure is associated with the tearing of the floor in correspondence to the top columns and top edge beam. This is a direct consequence of the chosen floor model which considers the sole contribution of the masonry blocks, which are characterized by a low tensile strength. In the present case the tensile contribution of the floor joists is not considered, thus resulting in a conservative estimation. In the RETROFIT scenario, the curves are initially elastic and then evolve limitedly in the nonlinear range. The failure is related to the development of a main crack in the diaphragm (Fig. 11). With respect to the AS-IS condition, as expected, the stiffness of the curve decreases as the tied arch span increases (Fig. 11), while capacity of the floor substantially decreases provided that the largest share of the in-plane action is transferred across the diaphragm to the new seismic resistant shear walls. It is worth noting that the lateral displacements at failure are very low in both cases: indeed, the maximum net deflection to span ratio at failure is negligible and corresponds to 1/14700 and 1/11400 for the AS-IS and RETROFIT scenario, respectively.

In addition, Fig. 10 shows in circles the capacity of the columns (i.e. the shear associated with the development of plastic hinges at the end of the columns in double bending considering a cross Sect. 30cm × 30cm, a longitudinal reinforcement ratio 0.88% and an inter-storey height 3m). After reaching the capacity, the columns are no longer effective in transferring the horizontal loads, therefore in the following analyses the stiffness contribution of the columns has been removed. This represents a lower bound of the floor capacity.

The results of the analyses highlight how possible problems to the diaphragm may arise after the seismic retrofit, leading to fragile failure mechanisms associated with tensile failure of the diaphragm at the midspan. For such reasons, additional analyses were carried out by adding a steel tie to the diaphragm, applied as an external stringcourse, with the purpose to increase the diaphragm capacity and ductility after the seismic retrofit. Figure 12 shows the results of these analyses including columns as elastic springs (grey dashed lines), for the reference case study, and without columns (blue, green and red lines for a floor shear capacity τ equal to 0.5 MPa, 0.9 MPa and 1.7 MPa, respectively). The steel tie

Fig. 10 Floor load vs net deflection at mid-span for the AS-IS and RETROFIT conditions. $\tau = 1.7$ MPa ($f_{ct} = 2.0$ MPa), $A_s = 5$ cm², $A_{Tie} = 0$ cm². Note: The right axis refers to horizontal floor acceleration in units of g. The horizontal dashed lines refer to the floor capacity as estimated in Sect. 3.3



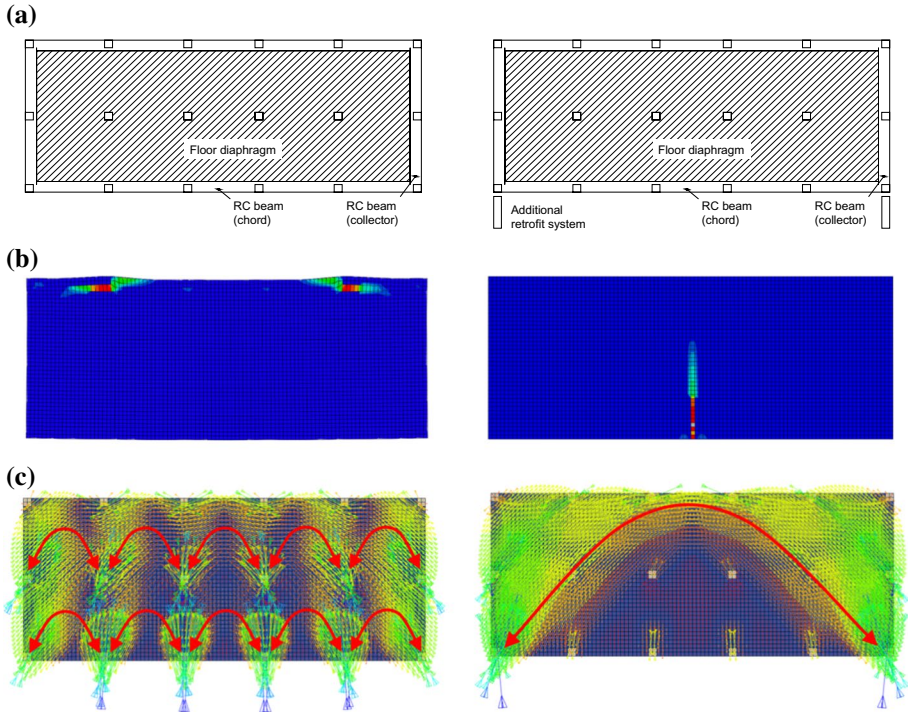


Fig. 11 **a** Scheme of the floor diaphragm displaying main components; **b** Qualitative plastic deformations at failure and **c** qualitative flow of the compression principal stresses (qualitative arches represented in red) for the AS-IS (left) and RETROFIT (right) conditions

was modelled with truss elements (B31 element in Abaqus) and pinned to the diaphragm edges in correspondence to the springs representing the additional retrofit system and to the diaphragm midspan. The same elastoplastic law adopted for the beam reinforcement was considered.

The results are similar, in qualitative terms, for the case with columns and without columns, although the latter condition is characterized by a lower capacity, as expected. It is worth noting that the in-plane floor resistance increases for increasing the additional tie cross-section as long as the failure is governed by Mechanism C. In the case of floors relying on a reduced amount of reinforcement in the longitudinal side beam and in the case of a small additional tie cross-section ($A_{Tie} = 5 \text{ cm}^2$), the collapse of the floor is associated with a crack propagating at the floor mid-span (Fig. 13a and Mechanism C in Fig. 5). For increasing values of the reinforcement area and thus of the additional tie stiffness and resistance, the failure mode changes from Mechanism C to Mechanism B, and the failure is reached for overcoming the shear resistance at the supports (Fig. 13b, c, and Mechanism B in Fig. 5). A further increase in the stringcourse cross-section does not change the floor in-plane resistance, which remains associated with Mechanism B, while it affects the stiffness of the system after the cracking onset of the side RC beam, as well as the crack width and the depth of the crack propagation at the mid-span. The onset of Mechanism B represents the maximum in-plane resource of the composite floor; further increase of the floor resistance would require strengthening of the slab or resorting to external diaphragms. In

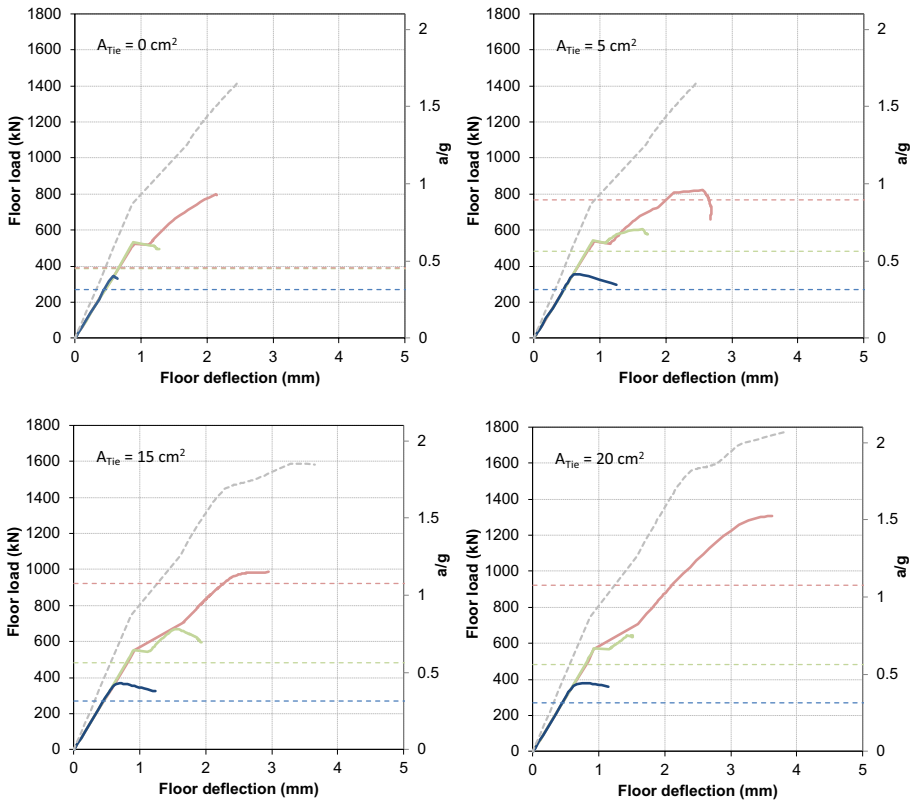


Fig. 12 Floor load vs net deflection at mid-span for varying tie cross sections and floor shear capacity. *Note:* the blue, green and red lines refer to a floor shear capacity τ equal to 0.5 MPa, 0.9 MPa and 1.7 MPa, respectively. The grey dashed line considers the presence of columns as elastic springs ($\tau = 1.7$ MPa, $A_s = 5$ cm²). The horizontal dashed lines refer to the floor capacity as estimated in Sect. 3.3. The right axis refers to horizontal floor acceleration in units of g

all the investigated cases, the maximum floor net deflection at the diaphragm's capacity is negligible, with a deflection to span ratio smaller than 1/6000. Therefore, the floor can be assumed as a fragile system with a very limited lateral net deflection capacity. Considering the effects of the diaphragm on the elastic lateral stiffness, it is worth noting that the ratio between the displacement at the centre of the diaphragm and at the diaphragm sides is equal to 1.03 and 1.35 without and with the additional shear walls, respectively. This confirms the fact that the floor in-plane stiffness is governed by the plan distribution of the lateral load vertical resisting system, i.e. by the boundary conditions. The floor in-plane stiffness affects the distribution of the horizontal seismic loading, but for the considered structural typology the main issue is the diaphragm capacity.

Figure 12 shows the influence of the diaphragm equivalent tensile strength as a function of the amount of steel tie cross-section. As expected, the reduction of the equivalent tensile strength leads to a reduction of the diaphragm load capacity. It is interesting to note that independently of the diaphragm tensile strength, a low amount of the tie cross-section does not provide benefits to the diaphragm load capacity, whereas when the tie cross-section is greater than 15 cm², the maximum load is bound to the shear capacity at

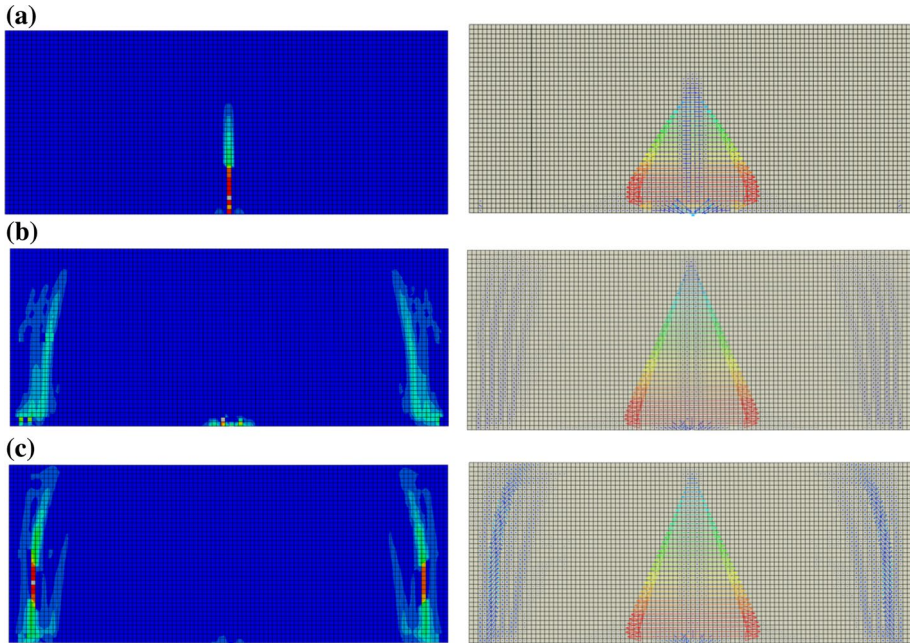


Fig. 13 Qualitative plastic deformations and plastic strain vectors at failure ($\tau = 1.7$ MPa) for: **a** $A_{Tie} = 5$ cm^2 , **b** $A_{Tie} = 15$ cm^2 , **c** $A_{Tie} = 25$ cm^2

the supports. It is also observed that low values of the tensile capacity are associated with low values of the floor net deflection (deflection to span ratios remaining always very low). Reference values for the floor capacity are shown in dashed horizontal lines for each value of τ (blue, green and red dashed lines refer to a floor shear capacity τ equal to 0.5 MPa, 0.9 MPa and 1.7 MPa). Such values have been determined according to Sect. 3.3 (with $\alpha_1 = \alpha_2 = 1$, $\beta = 1.3$, $b^* = 1320$ mm, $z_d = 8$ m, f_y taken as an average post yield value equal to 300 MPa). In the case of $\tau = 0.5$ MPa the floor capacity (269 kN) is governed by Mechanism B independently from the amount of tie reinforcement. In the case of $\tau = 0.9$ MPa, the floor capacity is governed by Mechanism C for $A_{Tie} = 0$ cm^2 and it is equal to 384 kN; for A_{Tie} greater or equal to 5 cm^2 the floor capacity is governed by Mechanism B and it is equal to 484 kN. In the case of $\tau = 1.7$ MPa, the floor capacity is governed by Mechanism C for $A_{Tie} = 0$ cm^2 and $A_{Tie} = 5$ cm^2 and it is equal to 384 kN and 768 kN, respectively; for $A_{Tie} = 15$ cm^2 and $A_{Tie} = 25$ cm^2 the floor capacity is governed by Mechanism B and it is equal to 915 kN. The results provide a conservative estimate of the floor capacity and allow to determine the governing failure mechanism.

5.2 Influence of floor openings

The influence of a stairwell opening was preliminary investigated for the RETROFIT condition considering both loading in the upward and downward directions. The presence of 2 additional shear walls in correspondence to the floor opening (Fig. 14a, right) was also analysed with the same overall retrofit system.

Figure 15 shows the results of the analyses in terms of floor load versus net deflection at mid-span for the various configurations. In the case of a floor opening and with a shear wall at each side of the floor (Fig. 14 left), the floor stiffness decreases as a consequence of the floor cross-section reduction at midspan while the floor strength is associated with the onset and the development of cracks at midspan. As expected, the resisting mechanism is characterized by the activation of arches with lower rise for the upward load compared to the downward load, as the resisting tied-arches adapt for the presence of the floor opening. As expected, the capacity is smaller in the case of downward load, as the arch tie is interrupted and the resisting arch is less constrained.

In the case of two additional shear walls in correspondence to the floor opening (Fig. 14 right), a significant increase of both the floor stiffness and strength is observed. The stiffness increase is associated with the reduction of the floor span between adjacent retrofit elements, while the strength increase is due to the presence of four additional walls, rather than two, despite the shear reaction force capacity remains unchanged. Furthermore, in this scenario, each resisting arch is effectively constrained at the supports. Figure 14 (right) shows the compressive arches that develops in the diaphragm. The floor capacity is associated with the onset of shear failure at the floor intermediate supports. Also in this case, the maximum floor net deflection at the diaphragm's capacity is low, with a net deflection to span ratio smaller than $1/5000$. Therefore, the floor can still be assumed as a fragile system with a very limited lateral deflection capacity. It is worth noting that the ratio between the

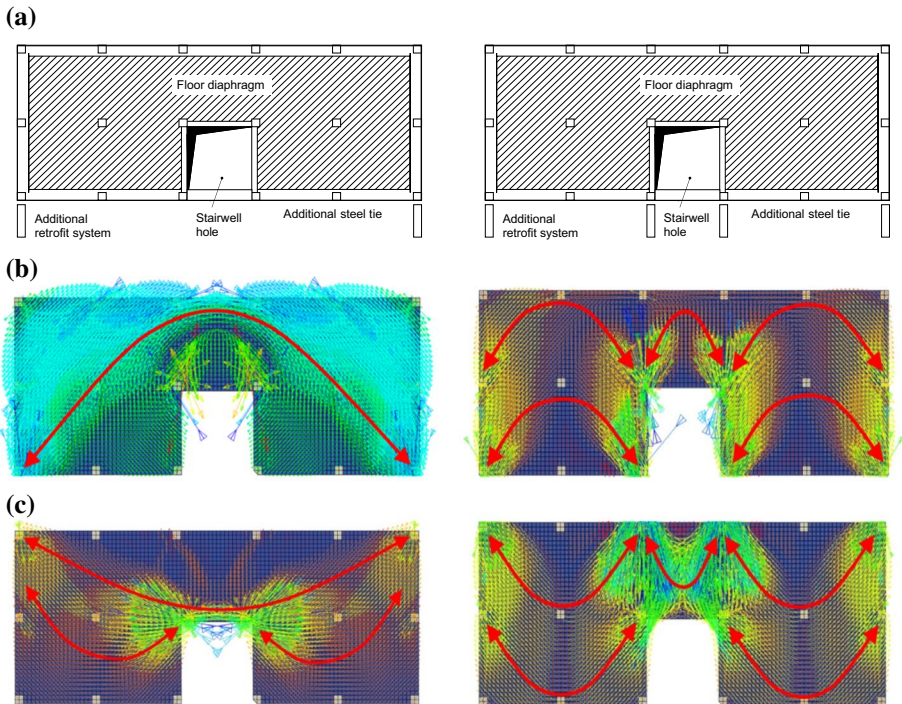
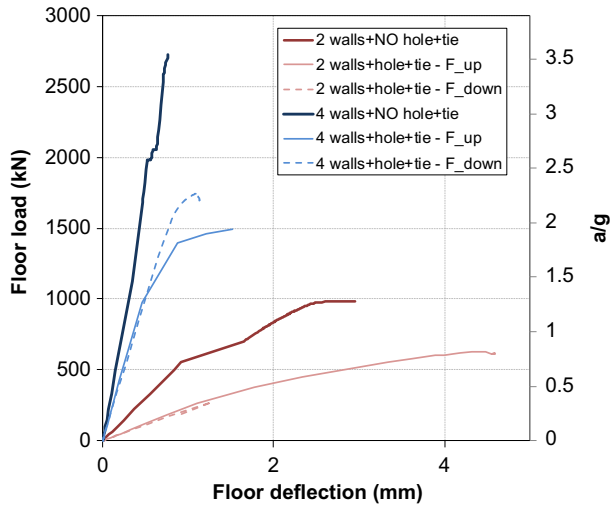


Fig. 14 Scheme of the floor diaphragm in the case of stairwell opening (a) and qualitative flow of the compression principal stresses with a downward (b) and upward (c) load. *Note:* the left and right figures represent the case of two shear walls and four shear walls, respectively. Qualitative arches are represented in red

Fig. 15 Floor load vs net deflection at mid-span in the case of stairwell opening. Note: The right axis refers to lateral acceleration in units of g for the stairwell hole conditions. $\tau = 1.7$ MPa ($f_{ct} = 2.0$ MPa); $A_s = 5$ cm²; $A_{tie} = 15$ cm². Stiffness of the columns not included



maximum displacement of the diaphragm at the mid span of the single or multiple bays and at its supports at the additional shear walls is equal to 1.89 and 1.11 in the case of two and four additional shear walls, respectively.

5.3 Influence of the side beam dimensions

Figure 16 shows the shear flow distribution along the interface between the side beam and the floor diaphragm for the RETROFIT condition by varying the dimensions of the side beam, thus by varying the ratio between the axial stiffness of the beam and the shear stiffness of the floor: 12cm×24cm (i.e. a RC floor joist), 30cm×60cm (i.e. a side beam), and 10 times the area of a side beam (i.e. to evaluate the limit behaviour for high axial stiffness of the side beam). The reference values of the floor material properties are considered. When the shear action transfer between the shear wall and the floor occurs at the edges, where side beams are expected, the axial stiffness of the side beam is much higher than the shear stiffness of the floor, therefore the shear stress distribution is wider and the maximum value of τ / τ_{mean} is 1.3. When new shear walls are introduced alongside the building in correspondence to a RC floor joist, rather than to a side beam, problems of shear stress diffusion might arise. In this case the reduction of the ratio between the axial stiffness of the joist and the shear stiffness of the floor causes a reduction in the distribution capacity of the joist, thereby introducing a substantial concentration of shear stresses close to the shear walls. In such conditions the maximum value of τ / τ_{mean} is 2.1. Such shear concentration could lead to an anticipated shear failure of the diaphragm. It is worth noting that this represents an ideal critical condition, indeed the RC edge beam will contribute to spread the concentrated load to more than one floor joist.

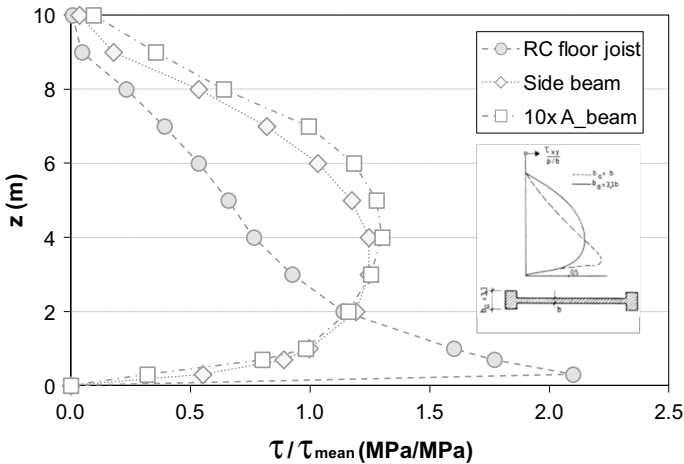


Fig. 16 Shear stress ratio (compared to the mean stress) along the lateral edge-beam of the floor as a function of the beam dimensions. Note: z is the depth of the floor. The graph on the right side represents the theoretical distribution (Leonhardt, 1979)

6 Design implications

The evaluation of the floor in-plane capacity can be conveniently used both for the seismic vulnerability assessment and for the conceptual design of the retrofit.

As previously discussed, the floor in-plane capacity is usually not the major problem in existing buildings in their “AS-IS” condition. In-plane failure of the floor was rarely observed after extensive field surveys carried out on non-seismic-conforming RC buildings after strong earthquakes, whereas common failure modes followed the onset of kinematic mechanisms in the frame associated with flexural and/or shear failure in some critical sections (Kaplan et al. 2010; Ricci et al. 2011). On the other hand, the floor capacity requires specific assessment in the case of retrofitted buildings. In this scenario, the floor in-plane capacity may become particularly critical in two cases: (1) the retrofit intervention increases the total stiffness of the building and no additional damping is provided, leading to a reduction of the structure fundamental period and consequently to an increase of the seismic actions transferred across the diaphragm; (2) the span of the resisting tied-arch increases up to the span between the elements of the new and stiffer lateral force resisting system, leading to higher internal actions and higher reaction forces at the tied-arch supports.

Accordingly, the actual floor in-plane capacity may influence the design of the retrofit interventions in two ways: (1) when the position of the additional lateral force resisting system is given, the in-plane floor capacity may be calculated as the minimum force triggering mechanisms A, B, and C (Sect. 3.3), and it enables determining whether strengthening of a selected floor is required, typically the upper floors, which are generally associated with the higher seismic loads (Mohele et al. 2010; Rodriguez et al. 2007), or the lower floors when ‘transfer functions’ of great magnitude are present due to displacement incompatibilities in the Lateral Force Resisting System (LFRS) or to discontinuities of the vertical elements of the LFRS (Gardiner et al. 2008); (2) when the position of the additional lateral force resisting system is to be defined, the in-plane floor capacity may enable determining the

maximum spacing between adjacent vertical elements of the new retrofit system (L_{SW}) to avoid the strengthening of the existing floors. For a given seismic action (f_s) and in-plane floor capacity (V_{fd}), such maximum distance is:

$$L_{SW} = \frac{2V_{fd}}{f_s} \tag{10}$$

When necessary, the floor strengthening may be attained by implementing different techniques. The first step of floor strengthening consists in the addition of a steel string-course along the floor perimeter in order to strengthen the arch tie and inhibit Mechanism C (Fig. 5). When Mechanism B (Fig. 5) dominates the floor capacity, a further increase of the steel stringcourse section does not entail a higher capacity of the floor, which needs to be strengthened (FEMA 547). In this case, “dry solutions”, such as intrados diaphragms made of steel truss-works, connected to the floor intrados or through post-tensioned tendons located at the ceiling level (Feroldi et al. 2013), may be adopted (Fig. 17a). These dry solutions entail minimum disruption of the building functions and could be concealed from sight with false ceilings. In the case of exoskeleton built with an offset with respect to the existing building (anytime new living spaces are introduced), new external diaphragms could be conceived in the gallery bridging the spacing of the new shear walls or the double skin cavities (Fig. 17b). Existing or new balconies can as well be re-engineered to act as external in-plane floor diaphragm (Fig. 17c). In these latter cases, the connections of the external diaphragm to the existing building must be guaranteed through post tensioned

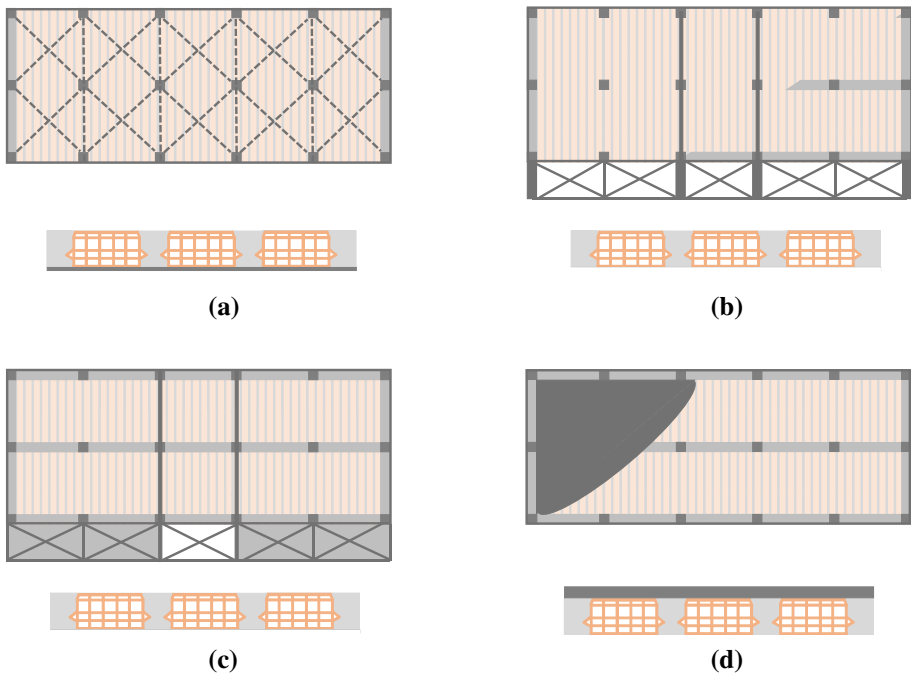


Fig. 17 Typical floor strengthening techniques: **a** intrados steel truss-work coverable by false ceilings; **b** external diaphragms bridging the spacing of new shear walls; **c** external diaphragms by reengineering existing or new balconies; **d** RC or HPRC overlay

tendons or special devices. Finally, more traditional solutions, such as fibre-reinforced polymer composite overlay or fibre RC topping overlay (Marini et al. 2010, Fig. 17d) with either normal strength or high-performance concrete may be adopted. However, such interventions require the demolition of the entire floor topping and finishing; in addition, they often entail high costs, disruption time, mandatory relocation of the occupants and possible disruption of the building functions during the construction works.

These new diaphragms share the in-plane load transfer with the existing diaphragm in proportion to the relative stiffness of the systems, which act as springs in parallel. It should be noted that with such an intervention, depending on the relative stiffness of the existing floor and the additional diaphragm, and thus on deformation compatibility, the crushing of the clay blocks may occur in any case, causing possible damage in the rooms beneath (Casprini et al. 2020). The resisting mechanism developing in the floors in the as-is condition and after the introduction of additional shear walls are reported in Fig. 18. On the right side of the figure, some details of the retrofit intervention are shown: the additional shear walls, the steel ring beam connected to the existing RC beam by means of studs, and the post-tensioned tendons or deep anchorages aimed at connecting the walls of the new LFRS to the existing structure.

7 Concluding remarks

The majority of the existing post-WWII building stock requires a deep retrofit intervention in order to fulfil the new requirements in terms of safety and sustainability. When seismic retrofit interventions are designed for existing buildings, regardless of the seismic strengthening technique, the floor diaphragm action is always required to transfer the floor inertial loads to the Lateral Force Resisting System (LFRS). The behaviour of the existing floors should thus be critically analysed in order to assess the building vulnerability and to design the structural retrofit intervention. This is particularly true for those retrofit techniques applied from the outside of the buildings since, in those cases, the need of existing floors

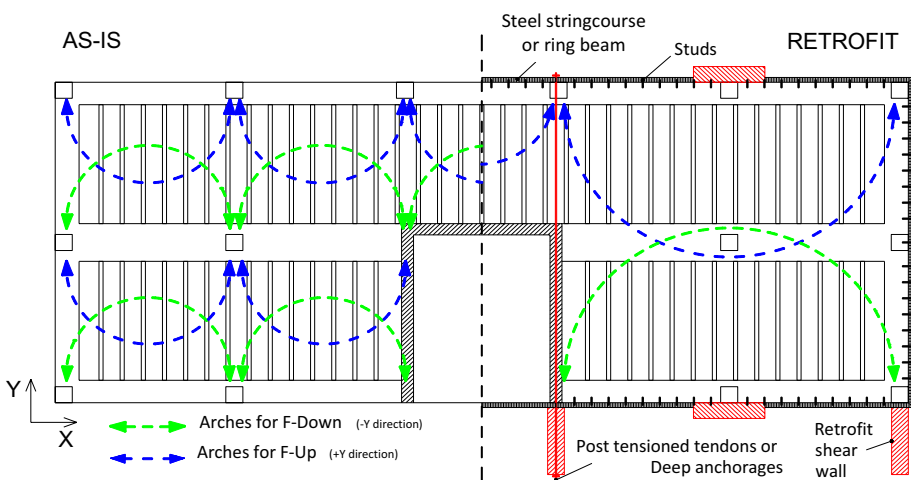


Fig. 18 Tied-arch system developing in the existing floors in the as-is condition (left side) and after the retrofit intervention (right side)

strengthening may require downtime of the building functions, and may hinder the entire retrofit project.

This study represents a first step of a major research investigating the in-plane response of existing RC beam-and-clay block floor systems; pivotal aim of the research is to put the focus on the assessment of the existing floor ability to act like a floor diaphragm in the case of a seismic event before and after major seismic retrofit interventions. The major findings of this study may be summarized as follow:

- The estimation of the diaphragm capacity is critical both for the vulnerability assessment of an existing RC building and for the conceptual design and the proportioning of the seismic retrofit intervention;
- In case of a regular geometry of the diaphragms, the in-plane capacity of the beam-and-clay block floor system is associated with the capacity of a tied-arch mechanism developing in the depth of the floor. The maximum capacity may be determined by the weakest mechanism (A, B, C in Fig. 5) that may either entail: A- the failure of the clay blocks at the arch key section; B- the failure at the tied-arched support; or C- the failure of the tied-arch bottom chord. The seismic force activating each of these mechanisms may be estimated as a function of the geometry of the floor (defining the geometry of the arch) and of the properties of the materials. Usually, the diaphragm capacity is associated with the onset of Mechanism B, which is the most critical and mainly depends on the ultimate shear resistance of the concrete topping (either plain or reinforced with a steel mesh, when present) and of the beam-and-block system. On the other hand, mechanism A, depending on the compression strength of the concrete slab and of the clay blocks, is usually activated for higher values of the seismic action, and Mechanism C, depending on the tensile capacity of the edge beam, despite being critical, may be easily inhibited by adding steel stringcourses along the beam perimeter (Fig. 18). It should be noted that, once the failure Mechanism B is activated, a further increase of the area of the stringcourse, which inhibits Mechanism C, does not lead to an increase of the diaphragm capacity and either floor strengthening or the addition of a new external diaphragm is required;
- The tied-arch resisting mechanism always develops in case of floors with concrete topping (Fig. 2a,c) either plain or reinforced with a steel mesh, and may develop also in the case of floors lacking the topping, as long as the clay hollow blocks extend over the entire thickness of the floor (Fig. 2b); on the contrary, when topping is lacking and blocks are constituted by an assemblage of clay tiles having no shear resistance (Fig. 2d), the floor does not exhibit any in-plane capacity and it always requires strengthening;
- When the dominating resisting mechanism is the tied-arch mechanism, i.e. in case of regular geometry of the floor and in absence of great openings that may affect the diaphragm flexibility, the behaviour of the diaphragm is brittle with limited lateral deflection capacity. In the numerical analyses, regardless of the considered scenario, the absolute value of the net deflection and the deflection to span ratios are considerably low. These results have been obtained from simplified numerical analyses, considering a floor with a regular rectangular geometry and modelling the beam-and-block system as an equivalent slab. However, preliminary results of both laboratory analyses carried out on a single block (Sect. 4) and in-situ experimental analyses carried out on a portion of an existing floor (Casprini et al. 2020) confirm such evidence.
- When addressing the role of the diaphragm in the seismic response of an existing or retrofitted building, it is fundamental to assess its structural conceptual design and its

ultimate capacity, even in relation to the floor layout and the related load paths. These major floor characteristics are fundamental to understand the behaviour of the diaphragm and should thus govern the design of the seismic retrofit interventions, allowing to define the need of the floor strengthening, the possibility to act from outside with seismic exoskeleton, and/or the maximum distance between the elements of the LFRS. Also, in case of openings and irregular geometry of the floor, additional transversal ties may be required to guarantee the development of an effectively constrained tied arch mechanism;

- When the strengthening of the floor is needed, dry techniques, solution applied at the intrados of the floor, or interventions from the outside (e.g. by re-engineering balconies or double skin cavities) should be preferred (Fig. 17a, b, c).

Ongoing developments of this research are associated with::

- The role and the relevance of the size and location of floor openings, as well as possible irregular floor layouts;
- The role of the ‘transfer forces’ (i.e. internal actions that develop in the diaphragms consequently to displacement incompatibilities or discontinuities of the vertical elements of the retrofit system) in the estimation of the internal load path and of the diaphragm seismic capacity;
- The study of the connections between the existing floor diaphragm and the new seismic resisting system, particularly when the new vertical elements of the lateral force resisting system are located only at the sides of the building (e.g. at the supports of Fig. 4) and the in-plane seismic action acts upwards (i.e. Figure 4, green lines);
- The role of the possible eccentricity between the centroid of the tie and the centre of pressure of the arch at the supports.

In-situ experimental tests on a wider portion of an existing beam-and-block floor system is also under development in order to validate the results of the experimental test carried out on the single block and to further investigating the mechanisms governing the in-plane behaviour of the floors. Preliminary results of such research are reported in Casprini et al. (2020).

Acknowledgements This research was partly carried out within the Italian national research project ReLUIS-DPC 2019–2021. The assistance of Eng. Valentina Zanotti during the experimental campaign is gratefully acknowledged.

Funding This research was partly carried out within the Italian national research project ReLUIS-DPC 2019–2021.

Availability of data and material The raw data supporting the conclusions of this article will be made available by the authors, upon reasonable requests.

Code availability Closed-source software was employed.

Declarations

Conflicts of interest The authors declare that the research was conducted in the absence of any commercial or financial relationships that could be construed as a potential conflict of interest.

Open Access This article is licensed under a Creative Commons Attribution 4.0 International License, which permits use, sharing, adaptation, distribution and reproduction in any medium or format, as long

as you give appropriate credit to the original author(s) and the source, provide a link to the Creative Commons licence, and indicate if changes were made. The images or other third party material in this article are included in the article's Creative Commons licence, unless indicated otherwise in a credit line to the material. If material is not included in the article's Creative Commons licence and your intended use is not permitted by statutory regulation or exceeds the permitted use, you will need to obtain permission directly from the copyright holder. To view a copy of this licence, visit <http://creativecommons.org/licenses/by/4.0/>.

References

- ANDIL, VV.AA. (1983). Il laterizio e la qualità del costruire, ANDIL-ASSOLATERIZI. (In Italian)
- Brandner R, Dietsch P, Dröscher J, Schulte-Wrede M, Kreuzinger H, Sieder M (2017) Cross laminated timber (CLT) diaphragms under shear: Test configuration, properties and design. *Constr Build Mater* 147:312–327
- Bull DK (2004) Understanding the complexities of designing diaphragms in buildings for earthquakes. *Bull N Z Soc Earthq Eng* 37(2):70–88
- Casprini E, Passoni C, Marini A, Belleri A, Giuriani E (2020) In-plane capacity of beam and block floor systems: an in-field experimental study. In: 17th International brick and block masonry conference (IB2MaC) from historical to sustainable masonry, 5–8 July 2020, Krakow, Poland
- Correal JF, Hidalgo V, Reyes JC et al (2020) A comparative study of seismic diaphragm design forces for RC dual system buildings. *Bull Earthquake Eng* 18:4515–4540
- Dassault Systèmes Simulia (2011) Abaqus User's Manual Version 6.11, Providence, RI, USA
- Di Lorenzo G, Colacurcio E, Di Filippo A, Formisano A, Massimilla A, Landolfo R (2020) State-of-the-art on steel exoskeletons for seismic retrofit of existing RC buildings. *Ingegneria Sismica* 37(1):50
- FEMA 547 (2006) Techniques for the seismic rehabilitation of existing buildings. Federal Emergency Management Agency, Washington, DC
- Feroldi F (2014) Riquilificazione sostenibile del patrimonio edilizio del secondo dopo guerra mediante doppia pelle ingegnerizzata per il rinforzo strutturale, l'efficientamento energetico e la riqualificazione architettonica e urbana. PhD thesis, University of Brescia (in Italian).
- Feroldi F, Marini A, Badiani B, Plizzari GA, Giuriani E, Riva P, Belleri A (2013) Energy efficiency upgrading, architectural restyling and structural retrofit of modern buildings by means of “engineered” double skin façade. In: Structures and architecture: concepts, applications and challenges—Proceedings of the 2nd international conference on structures and architecture, ICSA 2013, pp 1859–1866
- Fleischman RB, Naito CJ, Restrepo J, Sause R, Ghosh SK (2005a) Seismic design methodology for precast concrete diaphragms part 1: design framework. *PCI J*. <https://doi.org/10.15554/pci.09012005.68.83>
- Fleischman RB, Naito C, Restrepo J, Sause R, Ghosh SK, Wan G, Schoettler M, Cao L (2005b) Precast diaphragm seismic design methodology (DSDM) project, part 2: research program. *PCI J* 50(6):14–30
- Gardiner DR, Bull DK, Carr J (2008) Internal forces of concrete floor diaphragms in multistorey buildings. 2008 NZSEE Conference, Wairakei, New Zealand
- Giuriani E, Marini A (2008) Wooden roof box structure for the anti-seismic strengthening of historic buildings. *International Journal of Architectural Heritage* 2:226–246
- Giuriani E, Marini A, Preti M (2015) Thin folded shell for the renewal of existing wooden roofs. *Journal of Architectural Heritage* 10:797–816
- Iurcotta E (1968) *Costruzioni. Trattato teorico pratico*, Volume II, Signorelli. Milano. (in Italian)
- Kaplan H, Bilgin H, Yilmaz S, Binici H, Aztas A (2010) Structural damages of L'Aquila (Italy) earthquake. *Natural Hazards Earth Syst Sci* 10(3):499–507
- Labò S, Passoni C, Marini A, Belleri A (2020) Design of diagrid exoskeletons for the retrofit of existing RC buildings. *Engineering Structures*, 220:110899. 1 Oct 2020. DOI: <https://doi.org/10.1016/j.engstruct.2020.110899>
- León Flores GA, Lopez Batiz O, Padilla Romero DA (2008) Estudios experimentales del comportamiento sísmico de losas prefabricadas. XVI Congreso Nacional de Ingeniería Estructural. Veracruz, Ver., 2008. (in Spanish)
- Lourenco PB (1996) Computational strategies for masonry structures, PhD thesis, Delft University of Technology, Delft, The Netherlands
- Marini A, Passoni C, Belleri A, Feroldi F, Preti M, Metelli G, Giuriani E, Riva P, Plizzari G (2017) Combining seismic retrofit with energy refurbishment for the sustainable renovation of RC buildings: a proof of concept. *Eur J Environ Civ Eng*. <https://doi.org/10.1080/19648189.2017.1363665>
- Marini A, Plizzari G, Zanotti C (2010) Seismic enhancement of existing building by means of fiber reinforced concrete diaphragms. *J Civil Eng Arch* 4:6–15
- Matthews J (2005) Hollow-core floor slab performance following a severe earthquake. *Commer Rep. EQC* 99/411. University of Canterbury

- Mele E, Toreno M, Brandonisio G, De Luca A (2012) Diagrid structures for tall buildings: case studies and design considerations. *Struct Design Tall Spec Build* 23(2):124–145
- Milani G, Lourenço PB, Tralli A (2006a) Homogenization approach for the limit analysis of out-of-plane loaded masonry walls. *J Struct Eng* 132(10):1650–1663
- Milani G, Lourenço PB, Tralli A (2006b) Homogenised limit analysis of masonry walls, part II: structural examples. *Comput Struct* 84(3–4):181–195. <https://doi.org/10.1016/j.compstruc.2005.09.004>
- Moehle JP, Hooper JD, Kelly DJ, Meyer TR (2010) Seismic design of cast-in-place concrete diaphragms, chords, and collectors: a guide for practicing engineers. NEHRP Seismic design technical brief no. 3, produced by the NEHRP Consultants Joint Venture, a partnership of the Applied Technology Council and the Consortium of Universities for Research in Earthquake Engineering, for the National Institute of Standards and Technology, Gaithersburg, MD, NIST GCR 10–917–4
- Moghimi H, Driver RG (2013) Economical steel plate shear walls for low-seismic regions. *J Struct Eng* 139(3):379–388
- Moroder D. (2016). Floor diaphragms in multi-storey timber buildings. PhD thesis. University of Canterbury, Christchurch, New Zealand. March 2016
- Moroder D, Smith T, Pampanin S, Palermo A, Buchanan AH (2014c) Design of floor diaphragms in multi-storey timber buildings. *Int Netw Timber Eng Res*. Bath, England.
- NTC (2018) “Norme tecniche per le costruzioni”, D.M. 17 Gennaio 2018 (in Italian)
- Oliveto G, Liberatore L, Decanini LD (2011) Evoluzione storica della normativa sismica italiana alla luce degli effetti causati dal terremoto dell’Aquila del 2009. In Proceedings of: XVI ANIDIS conference, 18–22 september, Bari, Italy (in Italian)
- Passoni C, Guo J, Christopoulos C, Marini A, Riva P (2020) Design of dissipative and elastic high-strength exoskeleton solutions for sustainable seismic upgrades of existing RC buildings. *Eng Struct* 221:111057. <https://doi.org/10.1016/j.engstruct.2020.111057>
- Pecce M, Ceroni F, Maddaloni G, Iannuzzella V (2017) Assessment of the in-plane deformability of RC floors with traditional and innovative lightening elements in RC framed and wall structures. *Bull Earthq Eng* 15(7):3125–3149
- Pecce MR, Ceroni F, Maddaloni G (2019) In-plane deformability of RC floors: assessment of the main parameters and influence on dynamic behavior. *Bull Earthq Eng* 17:297–311
- Qu Z, Wada A, Motoyui S, Sakata H, Kishiki S (2012) Pin-supported walls for enhancing the seismic performance of building structures. *Earthquake Engng Struct Dyn* 41:2075–2091
- RDB VVAA (1950) Il Laterizio. Bollettino tecnico Erredibi, voll. I–V, RDB, Piacenza. (in Italian)
- Ricci P, De Luca F, Verderame GM (2011) 6th April 2009 L’Aquila earthquake, Italy: reinforced concrete building performance. *Bull Earthq Eng* 9(1):285–305
- Riva P, Perani E, Belleri A (2010) External R.C. structural walls for the repair of earthquake damaged buildings. In: Proceedings of Sustainable Development Strategies for Constructions in Europe and China, Rome. 19–20 Apr 2010
- Rodriguez ME, Restrepo JI, Blandón JJ (2007) Seismic design forces for rigid floor diaphragms in precast concrete building structures. *J Struct Eng ASCE* 133(11):1604–1615
- Schoettler MJ, Belleri A, Zhang D, Restrepo JI, Fleischman RB (2009) “Preliminary results of the shake-table testing for the development of a diaphragm seismic design methodology. *PCI J* 54(1):100–124
- Sustersic I, Dujic B (2014) Seismic Strengthening of Existing Concrete and Masonry Buildings with Crosslam Timber Panels. In: Aicher S et al. (eds), *Materials and Joints in Timber Structures*, RILEM Bookseries 9. Doi: https://doi.org/10.1007/978-94-007-7811-5_64
- Tena-Colunga A, Chinchilla-Portillo KL, Gelacio Juárez-Luna G (2015) Assessment of the diaphragm condition for floor systems used in urban buildings. *Eng Struct* 93:70–84
- United Nations (2015) Resolution adopted by the General Assembly on 25 September 2015 70/1. Transforming our world: The 2030 Agenda for Sustainable Development
- Zanni J, Cademartori S, Marini A, Belleri A, Giuriani E, Riva P, Angi B, Franchini G, Marchetti AL, Odorizzi P, Luitprandi G (2020) Riqualificazione integrata e sostenibile di edifici esistenti con esoscheletri a guscio prefabbricati: il caso studio AdESA. *Colloqui ATE. Nuovi orizzonti per l’architettura sostenibile*. Catania. (In Italian)
- Zanni J, Cademartori S, Marini A, Belleri A, Passoni C, Giuriani E, Riva P, Angi B, Brumana G, Marchetti AL (2021) Integrated deep renovation of existing buildings with prefabricated shell exoskeleton. *Sustainability* 13(20):11287. <https://doi.org/10.3390/su132011287>
- Zanotti V, Feroldi F, Marini A, Giuriani E (2014) Strengthening of RC buildings built after World War II: study of the behavior of existing floors in the presence of horizontal loads. Technical Report, DICATAM, University of Brescia, 2014. (in Italian)
- Zhang D, Fleischman RB (2016) Establishment of performance-based seismic design factors for precast concrete floor diaphragms. *Earthquake Engng Struct Dyn* 45:675–698

Publisher's Note Springer Nature remains neutral with regard to jurisdictional claims in published maps and institutional affiliations.

Authors and Affiliations

Alessandra Marini¹  · **Andrea Belleri**¹  · **Chiara Passoni**¹  · **Francesca Feroldi**² · **Ezio Giuriani**²

Alessandra Marini
alessandra.marini@unibg.it

Chiara Passoni
chiara.passoni@unibg.it

Francesca Feroldi
francesca.feroldi@unibs.it

Ezio Giuriani
ezio.giuriani@unibs.it

¹ University of Bergamo, Bergamo, Italy

² University of Brescia, Brescia, Italy